Supporting Information

Redox-Induced Molecular Actuators: The Case of Oxy-Alternate Bridged Cyclotetraveratrylene ($^{O\text{-}alt}$CTTV)

Saber Mirzaei, Denan Wang, Sergey V. Lindeman, Qadir K. Timerghazin*, and Rajendra Rathore*[†]

Department of Chemistry, Marquette University, Milwaukee, Wisconsin 53201-1881, United States
Email: denan.wang@marquette.edu; qadir.timerghazin@marquette.edu

[†]*Deceased February 16, 2018*

Contents

S1. General Methods and Synthesis

General methods: All commercial reagents were used without further purification unless otherwise noted. UV-vis absorption spectra were collected with an Agilent 8453 diode array spectrometer. Electronic absorption (UV-Vis/NIR) measurements were made on a Cary 5000 instrument. Cyclic and square-wave voltammograms were measured under inert atmosphere with an epsilon EC potentiostat (iBAS) at a scan rate of 100 mV/s with 0.1 M $[NBu_4]PF_6$ electrolyte. The three-electrode cell consisted of an Ag/AgCl reference electrode, a platinum auxiliary electrode, and a glassy carbon working electrode. All reactions for the synthesis of starting materials and the oxy-alternate bridged cyclo[*n*]veratrylenes (*n* = 4 ($^{O\text{-}alt}$CTTV) and *n* = 6 ($^{O\text{-}alt}$CHV)) were carried out under nitrogen atmosphere. NMR spectra were recorded on Varian 300 and 400 MHz NMR spectrometers. Mass spectra were recorded on Bruker Daltonics MALDI-TOF mass spectrometer, and dithranol was used as matrix. The oxy-bridged veratrole dimer (Bis(3,4-dimethoxyphenyl)ether) is synthesized using the previously reported method.[1] Midwest Micro Lab, LLC, Indianapolis, Indiana 45250, performed all elemental analyses.

$^{O\text{-}alt}$CTTV and $^{O\text{-}alt}$CHV synthesis: To a solution of oxygen-bridged veratrole dimer (Bis(3,4-dimethoxyphenyl)ether) (4 mmol, 1.2 g) in chloroform ($CHCl_3$, 40 ml), paraformaldehyde was added (0.24 g, 8 mmol, 2.0 eq) under the nitrogen atmosphere. Then, the methanesulfonic acid (CH_3SO_3H, 0.1 ml, 0.15 mmol) was added and the mixture was stirred at the room temperature for 5 h. The reaction has been quenched by adding water (40 ml) to the Schlenk flask and letting it stir vigorously for 30 min. The organic layer has been separated using the separatory funnel and the $CHCl_3$ has been evaporated under the vacuum. The product has been purified by column chromatography using pure chloroform to obtain the white solid for both $^{O\text{-}alt}$CTTV (0.9 g, yield = 70%) and $^{O\text{-}alt}$CHV (0.1 g, yield = 8%). The pure products have been confirmed using the ^{1}H-NMR, ^{13}C-NMR and MALDI-TOF spectroscopy techniques. Moreover, the crystal structure of $^{O\text{-}alt}$CTTV (using slow evaporation method by employing 5:2 mixture of $CHCl_3$/MeOH solvents at room temperature) is reported.

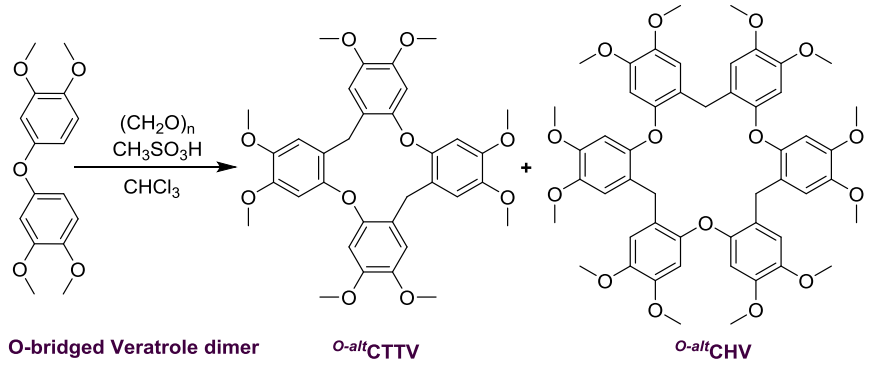

Cyclotetraveratrylene ($^{O\text{-}alt}$CTTV): white solid; *mp* = 275-277 °C; ^{1}H NMR (20 °C, $CDCl_3$) δ = 6.79 (s, 4H), 6.40 (s, 4H), 4.34 (s, 2H), 3.85 (s, 12H), 3.72 (s, 12H), 3.15 (s, 2H); ^{13}C NMR (20 °C, $CDCl_3$) δ = 148.04, 144.76, 123.70, 114.24, 102.79, 56.63, 56.17, 29.17. Calcd for $C_{34}H_{36}O_{10}$: C, 67.54; H, 6.00. Found: C, 67.61; H, 6.03.

Cyclohexaveratrylene ($^{O\text{-}alt}$CHV): white solid; *mp* = 204-206 °C; ^{1}H NMR (20 °C, $CDCl_3$) δ = 6.61 (s, 6H), 6.17 (s, 6H), 3.82 (s, 6H), 3.76 (s, 18H), 3.64 (s, 18 H); ^{13}C NMR (20 °C, $CDCl_3$) δ = 149.02, 148.03, 144.66, 122.89, 113.87, 102.93, 56.59, 56.11, 29.11. Calcd for $C_{51}H_{54}O_{15}$: C, 67.54; H, 6.00. Found: C, 67.44; H, 6.00.

S2. ^{1}H- and ^{13}C-NMR Spectra

^{1}H-NMR of (Bis(3,4-dimethoxyphenyl)ether) oxy-bridged veratrole dimer ($CDCl_3$, 20 °C)

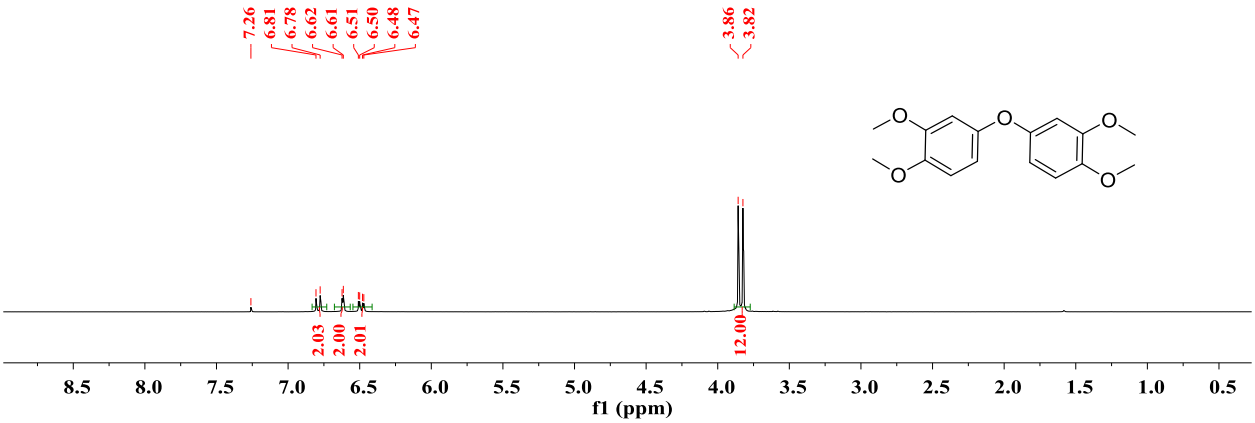

^{13}C-NMR of (Bis(3,4-dimethoxyphenyl)ether) oxy-bridged veratrole dimer ($CDCl_3$, 20 °C)

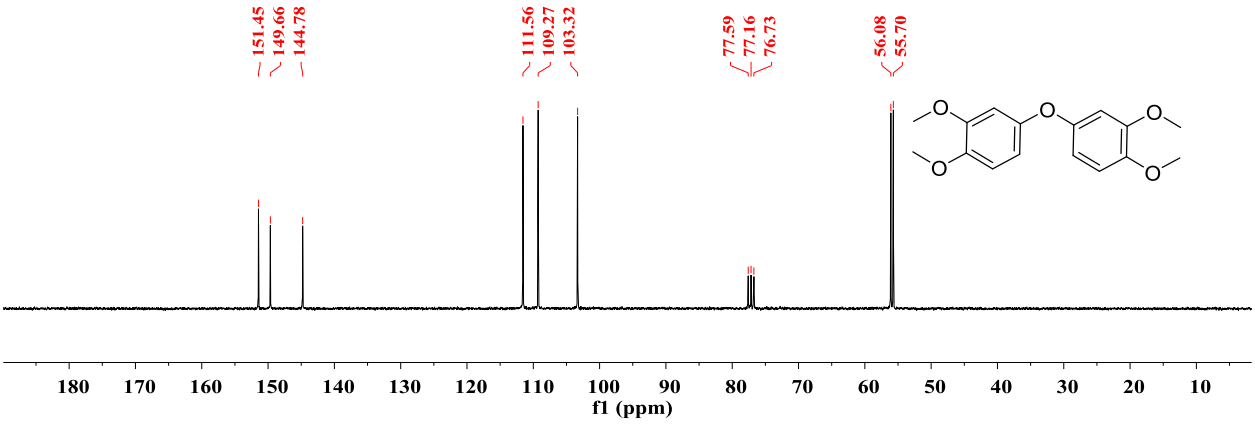

^{1}H-NMR of $^{O\text{-}alt}$CTTV ($CDCl_3$, 20 °C)

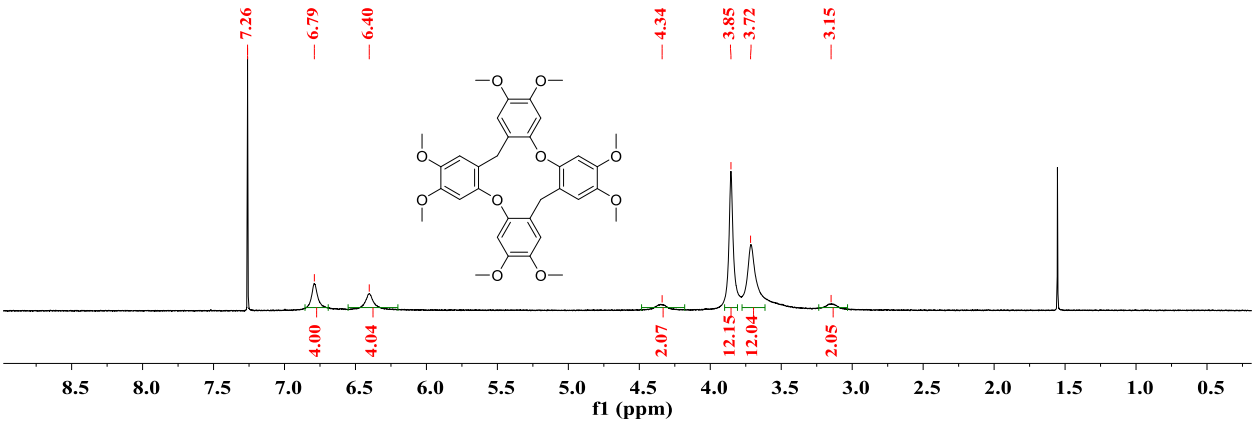

^{13}C-NMR of $^{O\text{-}alt}$CTTV ($CDCl_3$, 20 °C)

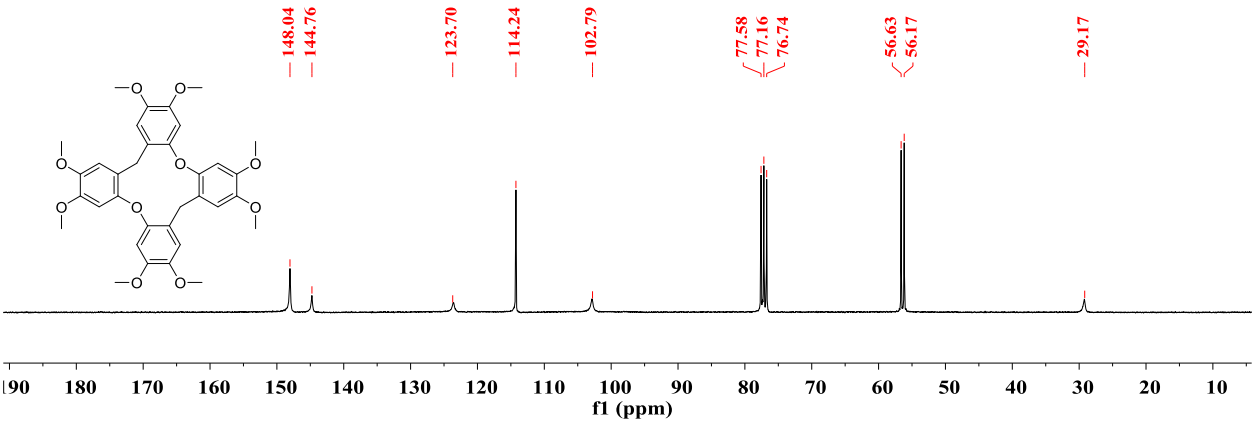

^{1}H-NMR of $^{O\text{-}alt}$CTTV (CD_2Cl_2, 20 °C)

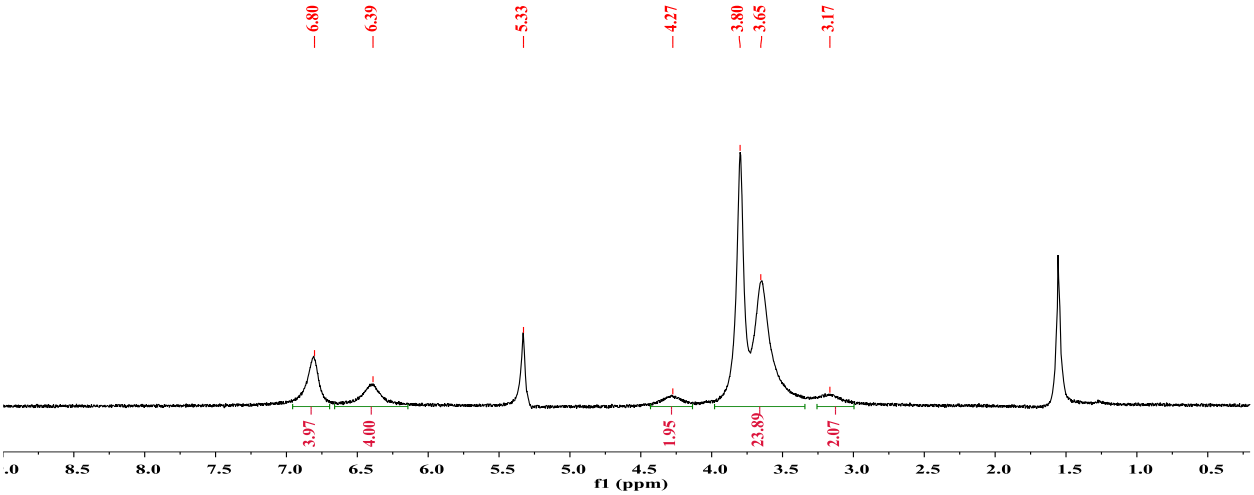

Figure S1. Comparing NMR spectra of $^{O\text{-}alt}$CTTV in CD_2Cl_2 (20 °C) and $CDCl_3$ (20 °C)

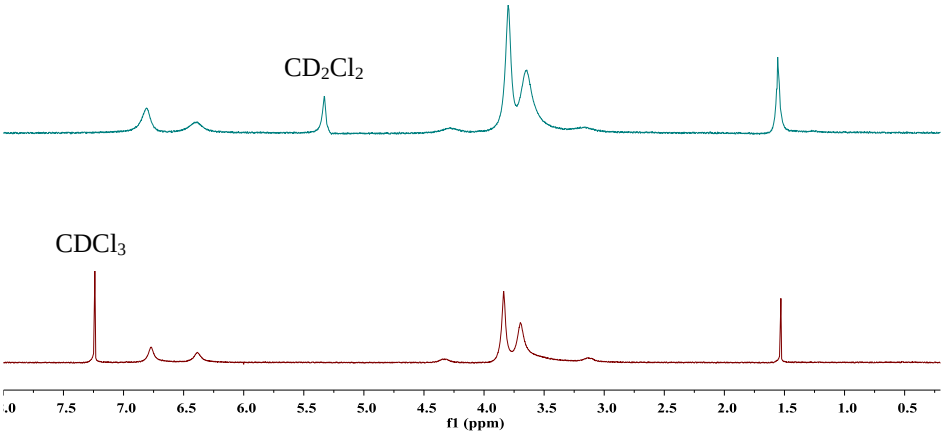

^{1}H-NMR of $^{O\text{-}alt}$CHV ($CDCl_3$, 20 °C)

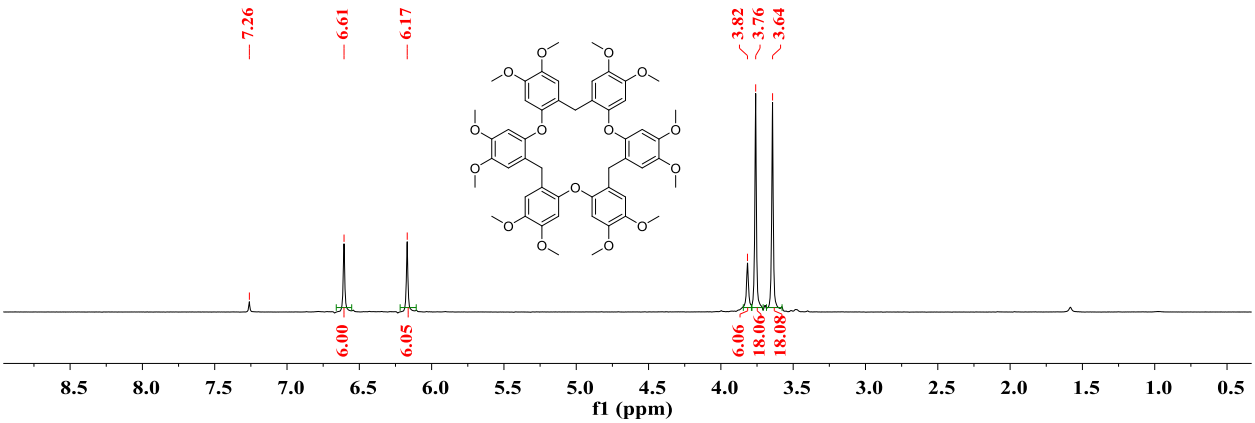

^{13}C-NMR of $^{O\text{-}alt}$CHV ($CDCl_3$, 20 °C)

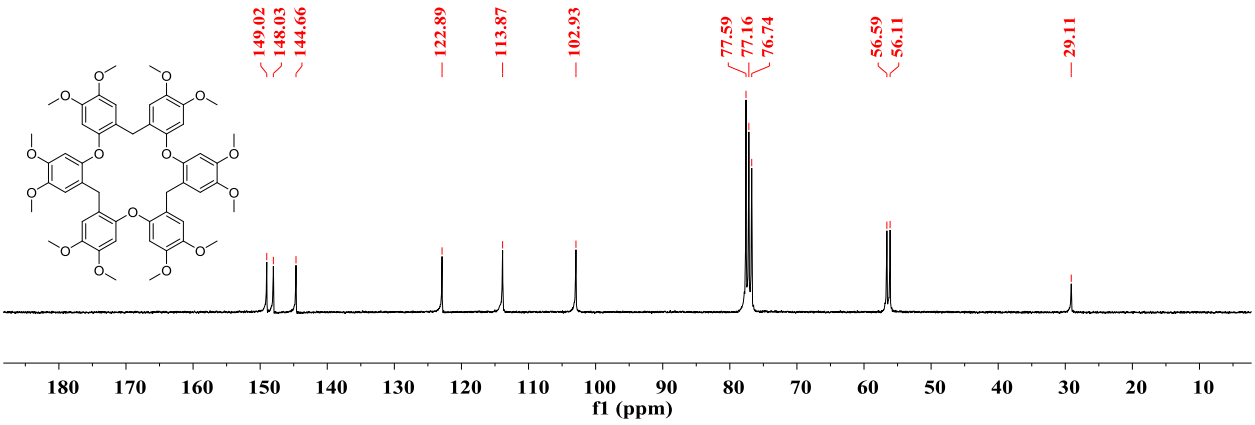

Variable temperature ^{1}H-NMR of $^{O\text{-}alt}$CTTV (from 55 °C to -50 °C in $CDCl_3$ solvent)

Figure S2. Variable temperature (VT) NMR of $^{O\text{-}alt}$CTTV in $CDCl_3$ in the range from 55 to -50 °C.

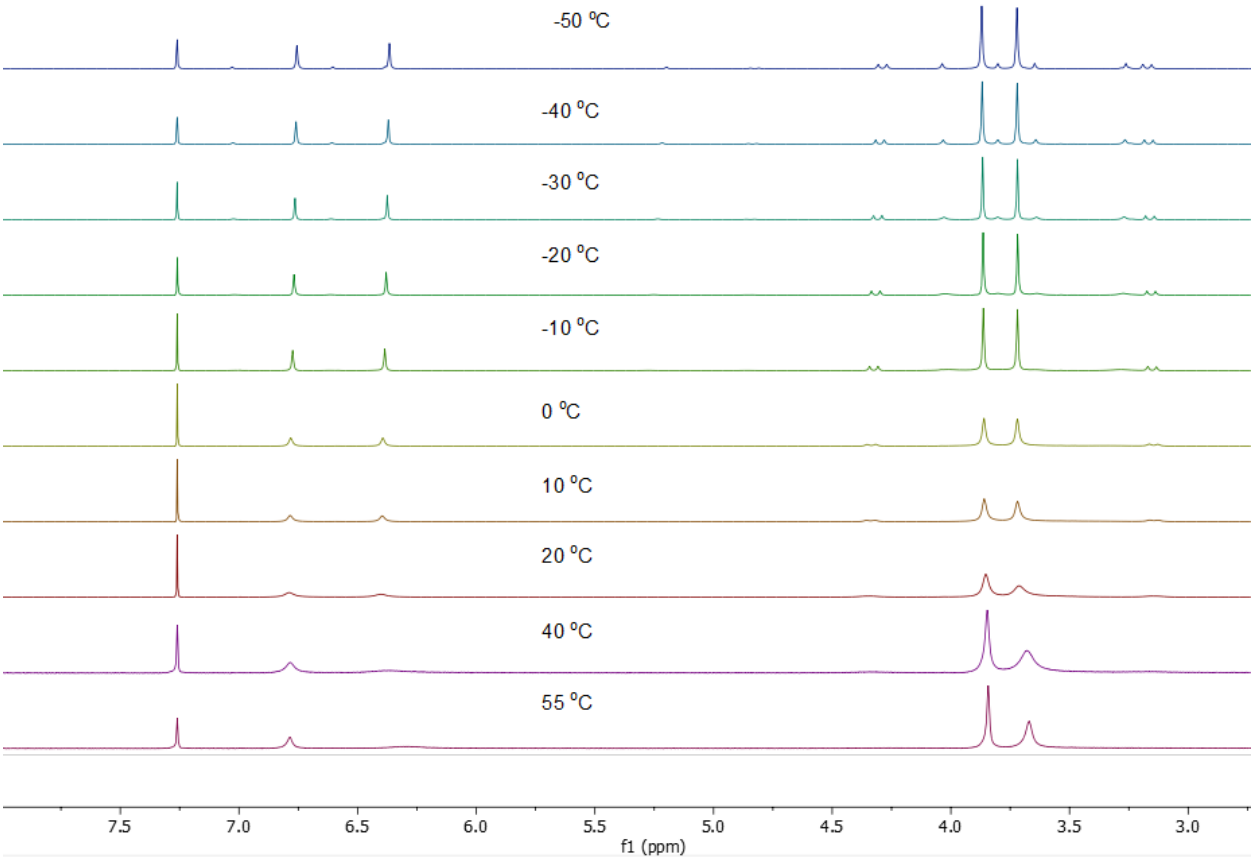

^{1}H-NMR of $^{O\text{-}alt}$CTTV ($CDCl_3$, -50 °C)

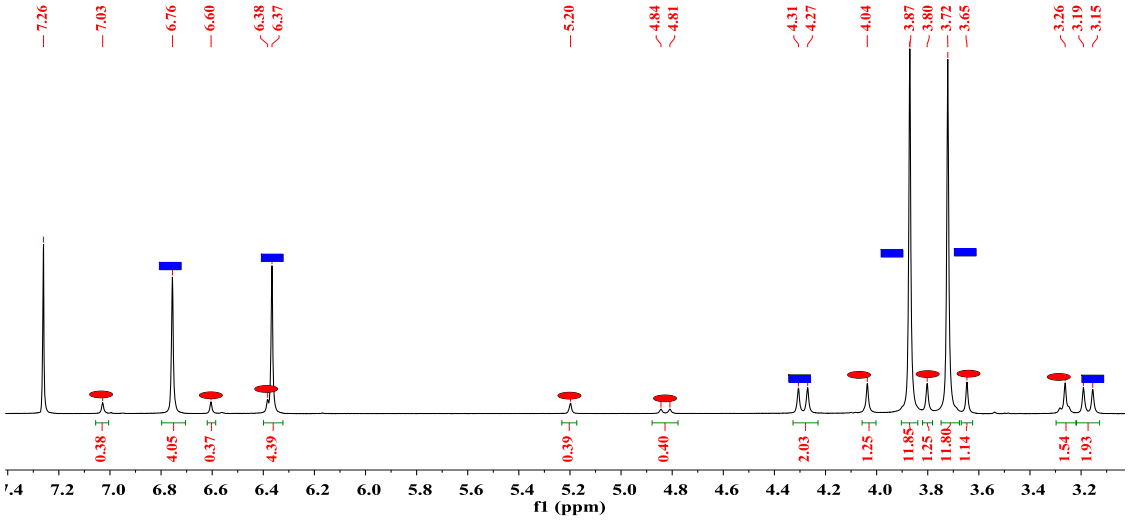

Figure S3. Comparing NMR spectra of $^{O\text{-}alt}$CTTV; reduction product with Zn powder and neutral THEO in $CDCl_3$.

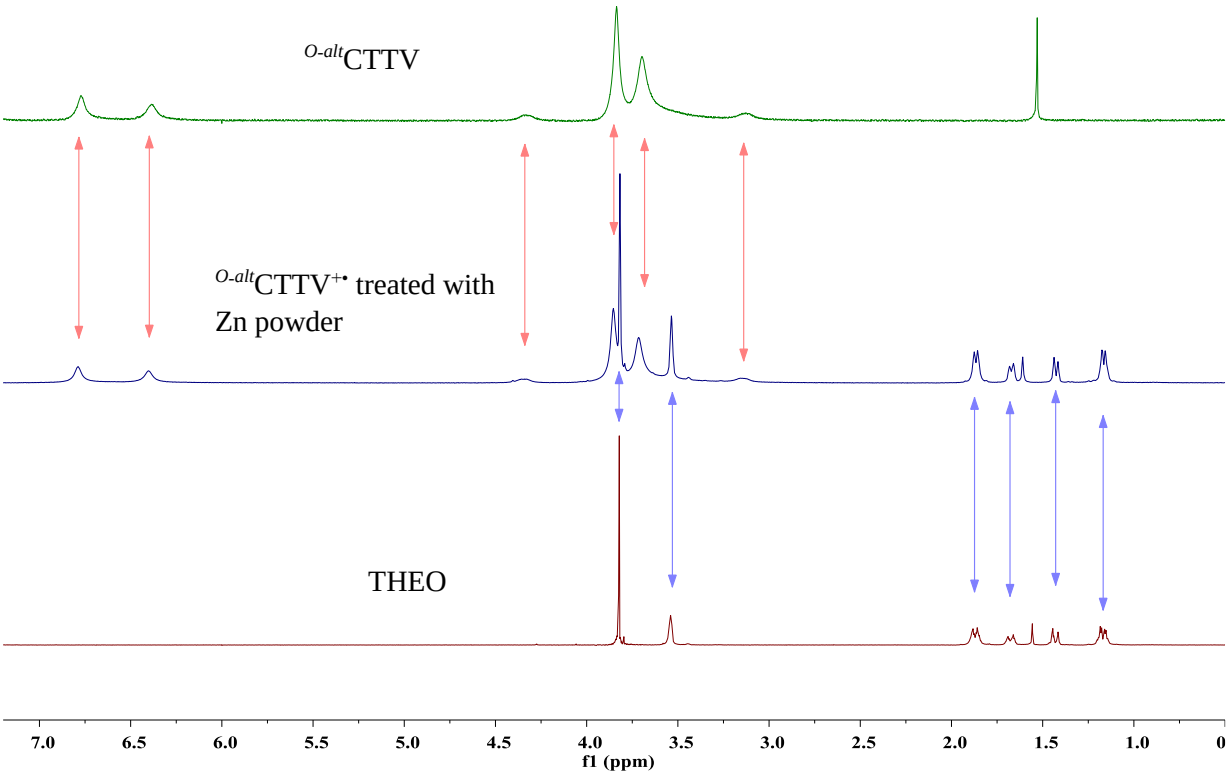

S3. MALDI-TOF Data

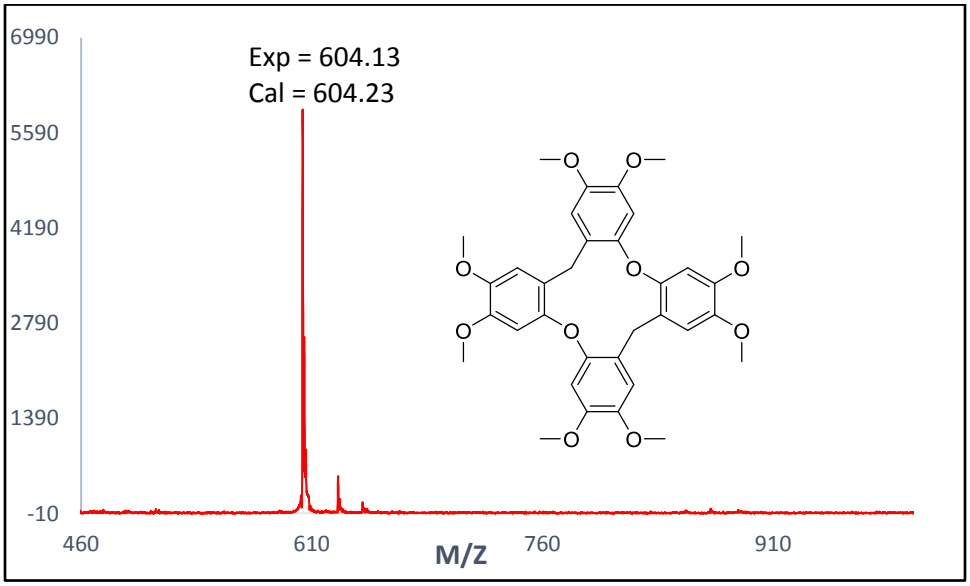

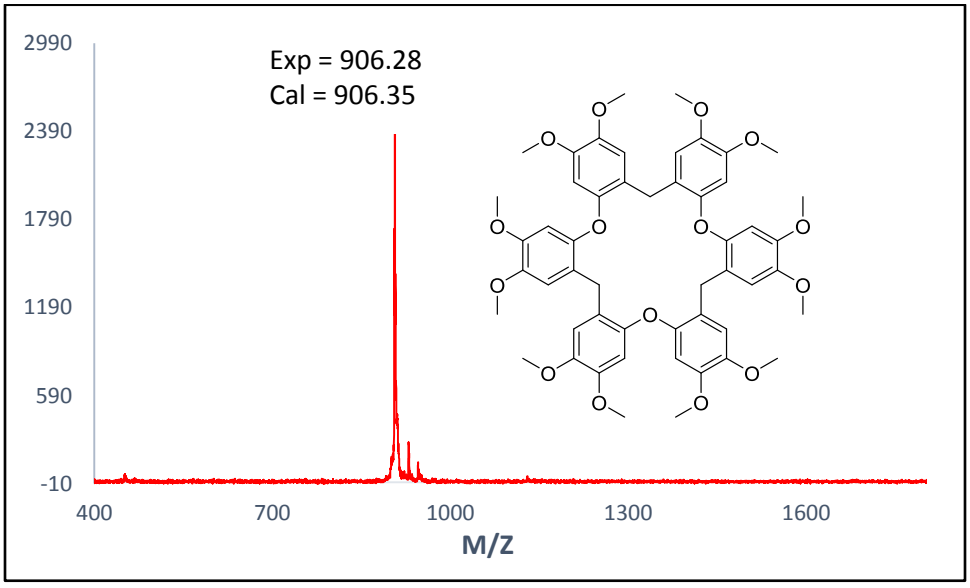

S4. Electrochemical Characterization of $^{O\text{-}alt}$CTTV

Figure S4. Cyclic voltammogram (CVs, solid line) and square wave (SW, dashed line) of 2 mM $^{O\text{-}alt}$CTTV in CH_2Cl_2 (0.1 M n-Bu_4NPF_6) at a scan rate 100 mV s^{-1} (V vs. Fc/Fc^+).

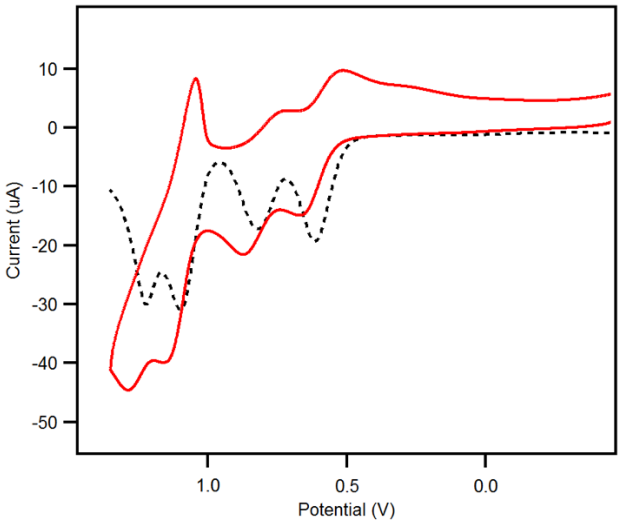

S5. Generation of $^{O\text{-}alt}$CTTV$^{+\bullet}$ by Redox Titrations

Electronic absorption spectra of $^{O\text{-}alt}$**CTTV**$^{+\bullet}$ in CH_2Cl_2 at 22 °C were obtained by quantitative redox titrations using robust aromatic oxidant, *i.e.*, [**THEO**$^{+\bullet}$$SbCl_6^-$] (1,4:5,8-dimethano-1,2,3,4,5,6,7,8-octahydro-9,10-dimethoxyanthracene hexachloroantimonate; E_{red1}= 0.67 V vs Fc/Fc^+, λ_{max}= 518 nm, λ_{max}= 7300 cm^{-1} M^{-1}).

Figure S5. Chemical structures of aromatic oxidant **THEO** used in redox titrations.

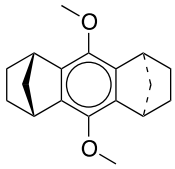

THEO

The redox titration experiment has been carried out by an incremental addition of $^{O\text{-}alt}$**CTTV** to the solution of **THEO**$^{+\bullet}$ where the 1-e^- oxidation of $^{O\text{-}alt}$**CTTV** and reduction of **THEO**$^{+\bullet}$ can be described by equilibrium equation:

$$\textbf{THEO}^{+\bullet} + {}^{O\text{-}alt}\textbf{CTTV} \rightleftarrows \textbf{THEO} + {}^{O\text{-}alt}\textbf{CTTV}^{+\bullet} \quad \text{(eq. 1)}$$

Numerical deconvolution of the absorption spectrum at each increment produced mole fractions of **THEO**$^{+\bullet}$ and $^{O\text{-}alt}$**CTTV**$^{+\bullet}$ against the added equivalents of $^{O\text{-}alt}$**CTTV** and confirmed a 1:1 stoichiometry of the redox reaction (**Figure S6** below reproduced from **Figure 4** in the main text). The experimental plots of mole fraction vs equivalent of added donor were fitted by varying $\Delta G_1 = E_{ox1}^{o-alt\boldsymbol{CTTV}} - E_{red}^{\textbf{THEO}^{+\bullet}}$.

Figure S6. Left: Spectral changes attendant upon the oxidation of $^{O\text{-}alt}$**CTTV** (1.98 mmol) by **THEO**$^{+\bullet}$**SbCl6**$^-$ (0.140 mmol) in CH_2Cl_2 at 22 ºC. Right: Red, green and blue curves correspond to the absorbance at indicated wavelength (nm) against number of equivalents of added $^{O\text{-}alt}$**CTTV**.

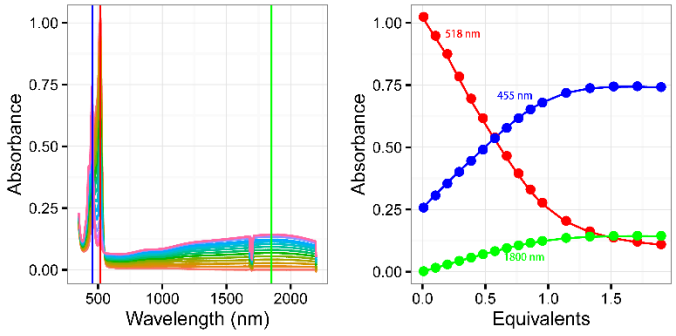

S6. X-Ray Crystallography Data

Table S1. Summary of X-ray crystallographic data collection and structure refine.

Identification code	kad1k	kad1p
Empirical formula	$C_{39}H_{41}Cl_{15}O_{10}$	$C_{36}H_{40}Cl_{10}O_{10}Sb$
Formula weight	1201.47	1108.93
Temperature/K	100.2(8)	100.00(10)
Crystal system	triclinic	orthorhombic
Space group	P-1	Pbcn
a/Å	12.3355(3)	30.6757(3)
b/Å	13.4478(4)	15.72509(18)
c/Å	16.8786(5)	23.3903(3)
α/°	101.227(2)	90
β/°	107.842(2)	90
γ/°	99.924(2)	90
Volume/Å^3	2532.27(13)	11282.9(2)
Z	2	8
ρ_{calc}g/cm^3	1.576	1.306
μ/mm^{-1}	7.912	8.594
F(000)	1220.0	4456.0
Crystal size/mm^3	0.816 × 0.388 × 0.25	0.466 × 0.173 × 0.083
Radiation	CuKα (λ = 1.54184)	CuKα (λ = 1.54184)
2Θ range for data collection/°	6.918 to 141.402	7.362 to 141.254
Index ranges	$-15 \le h \le 15$, $-16 \le k \le 16$, $-19 \le l \le 20$	$-36 \le h \le 37$, $-18 \le k \le 15$, $-28 \le l \le 28$
Reflections collected	45934	54883
Independent reflections	9609 [R_{int} = 0.0574, R_{sigma} = 0.0324]	10692 [R_{int} = 0.0430, R_{sigma} = 0.0239]
Data/restraints/parameters	9609/12/505	10692/0/522
Goodness-of-fit on F^2	1.100	1.046
Final R indexes [I>=2σ (I)]	R_1 = 0.0872, wR_2 = 0.2656	R_1 = 0.0618, wR_2 = 0.1883
Final R indexes [all data]	R_1 = 0.0914, wR_2 = 0.2690	R_1 = 0.0700, wR_2 = 0.1965
Largest diff. peak/hole / e Å^{-3}	0.94/-0.54	1.09/-1.24

Figure S7. The ORTEP diagrams (50% probability) of $^{O\text{-}alt}$CTTV in neutral (left) and cation radical state (right). The hydrogen atoms and solvents molecules are omitted for clarity.

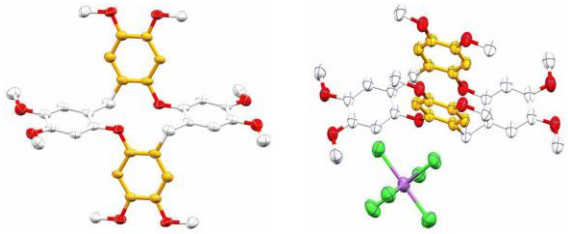

Table S2. The bond length (in picometers, pm) analysis of neutral and cation state of $^{O\text{-}alt}$CTTV crystal structures.

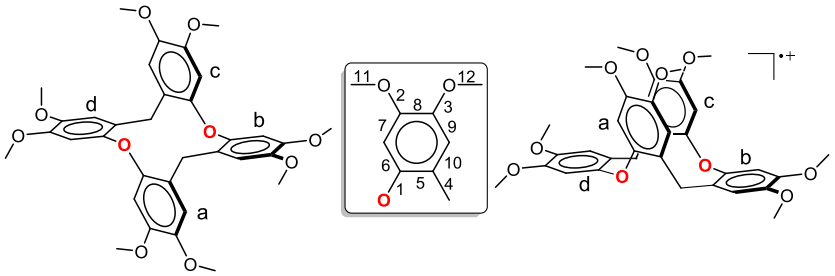

3	a				b				c				d			
bond	open-1	open-2	Closed$^{\bullet+}$	Δ^a	open-1	open-2	Closed$^{\bullet}$	Δ^a	open-1	open-2	Closed$^{\bullet}$	Δ^a	open-1	open-2	Closed$^{\bullet}$	Δ^a
1	138	139.1	135.3	-3.2	139.1	138.7	140.8	1.9	138	139.1	139.1	0.55	139.1	138.7	140.7	1.8
2	136.5	136.7	133.4	-3.2	137.5	137.3	137.7	0.3	136.5	136.7	136.5	-0.1	137.5	137.3	136.1	-1.3
3	137.8	138.1	133.2	-4.8	136.9	134.8	136.2	0.35	137.8	138.1	137.8	-0.15	136.9	134.8	136.8	0.95
4	150.2	152.6	151.5	0.1	151.2	152.1	152.4	0.75	150.2	152.6	152.1	0.7	151.2	152.1	152.4	0.75
5	139.8	137.5	141.9	3.3	138.3	138.6	137.4	-1.05	139.8	137.5	140	1.35	138.3	138.6	137.4	-1.05
6	139.8	140.7	139.1	-1.2	139.2	139.7	138.1	-1.35	139.8	140.7	140.1	-0.15	139.2	139.7	138.3	-1.15
7	137.6	139.1	138.2	-0.2	137.7	137.6	138.6	0.95	137.6	139.1	137.4	-0.95	137.7	137.6	138.2	0.55
8	139.9	140	142.4	2.45	141.3	141.9	139.7	-1.9	139.9	140	140.6	0.65	141.3	141.9	140.3	-1.3
9	137.2	137.9	139.5	1.95	138.2	139.4	138.9	0.1	137.2	137.9	136.4	-1.15	138.2	139.4	138.8	0
10	141.6	139.5	136	-4.6	140.4	139.3	140.4	0.55	141.6	139.5	139.6	-0.95	140.4	139.3	140.2	0.35
11	143.6	142.6	144.2	1.1	142.1	143.6	142.6	-0.25	143.6	142.6	142.3	-0.8	142.1	143.6	144.1	1.25
12	142.8	140.8	145.7	3.9	142.9	142.6	143.3	0.55	142.8	140.8	141.5	-0.3	142.9	142.6	141.9	-0.85

[a] Δ = closed$^{\bullet+}$ - (open-1+open-2)/2

Figure S8. The graphical representations of bond length changes (ΔR = closed$^{\bullet+}$ - open) of $^{O\text{-}alt}$CTTV crystal structures in picometers (pm).

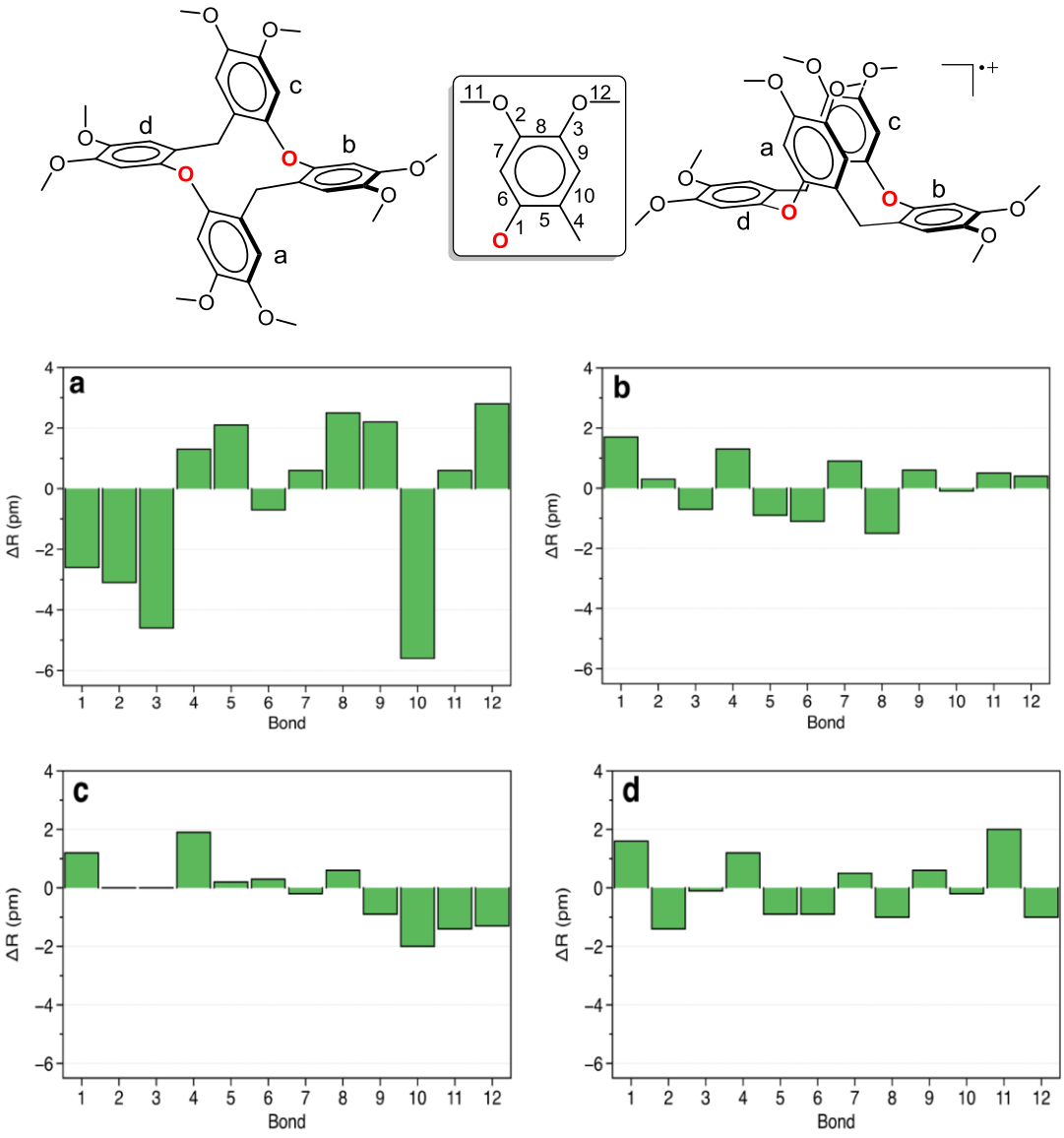

S7. Computational Details

All calculations were carried out using Gaussian 16 software package.[2] Two long-range corrected (ωB97XD and CAM-B3LYP) and one meta-GGA (M06-2X) hybrid functionals of density functional theory (DFT) are used for all optimizations and subsequent spectroscopy studies.[3-5] In order to include the dispersion effects, the D3 version of Grimme with Becke-Johnson damping factors (D3BJ) are used for the CAM-B3LYP functional.[6] The double-zeta quality basis set include diffuse and polarization functions on heavy atoms and polarization functions on hydrogens (6-31+G(d,p), BS1) is used for all calculations. Moreover, for the sake of accuracy, the single point energy calculations have been carried out for all of the fully optimized structures using double-hybrid B2PLYPD3 functional.[7] This double hybrid functional benefits from using 53% HF exchange and 27% MP2 correlation which showed very reliable energies and low spin contamination for the open shell systems.[8] These single point calculations were done using bigger basis set (6-311++G(2d,2p), BS2). The implicit solvation effects are included using the integral equation formalism variant of the polarizable continuum model (IEF-PCM) with standard parameters of chloroform ($CHCl_3$).[9] Moreover, in order to investigate the effect of implicit solvent polarity on the relative stability of the $^{O\text{-}alt}$CTTV$^{\bullet+}$ conformers, the calculations are repeated by employing three more solvents (dichloromethane, acetonitrile, methanol) at the ωB97XD/BS1 level of theory. The gauge-independent atomic orbital (GIAO) method[10] is used for ^{1}H NMR chemical sift calculations using the ωB97XD functional and BS1. The calculated chemical shieldings are scaled with ^{1}H NMR chemical shift of Tetramethylsilane (TMS, 31.67 ppm) calculated at the ωB97XD/BS1+PCM($CHCl_3$) level of theory. The spin density distributions were calculated using the natural bond orbital approach using integrated NBO 3.1 code in Gaussian 16 package.[11] The analysis of TDDFT studies have been carried out using the GaussSum 3.0 software package.[12]

Table S3. The experimental (X-ray) and computational (ωB97XD/BS1-PCM($CHCl_3$)) bond length of one of the cofacial rings of $^{O\text{-}alt}$CTTV in its neutral and cation radical states in picometers (pm).

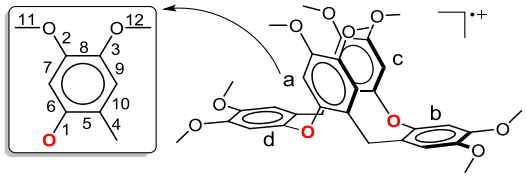

	DFT			X-ray		
bond	open	closed$^{\bullet+}$	Δ^a	open	closed$^{\bullet+}$	Δ^a
1	138.2	133.0	-5.1	138.0	135.3	-2.6
2	135.6	131.6	-4.0	136.5	133.4	-3.1
3	136.1	131.5	-4.6	137.8	133.2	-4.6
4	151.7	151.0	-0.8	150.2	151.5	1.3
5	138.7	144.1	5.4	139.8	141.9	2.1
6	140.0	139.4	-0.6	139.8	139.1	-0.7
7	138.8	138.4	-0.4	137.6	138.2	0.6
8	141.2	145.3	4.1	139.9	142.4	2.5
9	138.6	139.9	1.3	137.2	139.5	2.2
10	140.3	137.9	-2.5	141.6	136.0	-5.6
11	141.6	143.2	1.6	143.6	144.2	0.6
12	141.5	143.4	1.9	142.8	145.7	2.8

$^a\Delta$ = closed$^{\bullet+}$ - open

Figure S9. The 3-D representation of possible conformers of $^{O\text{-}alt}$CTTV.

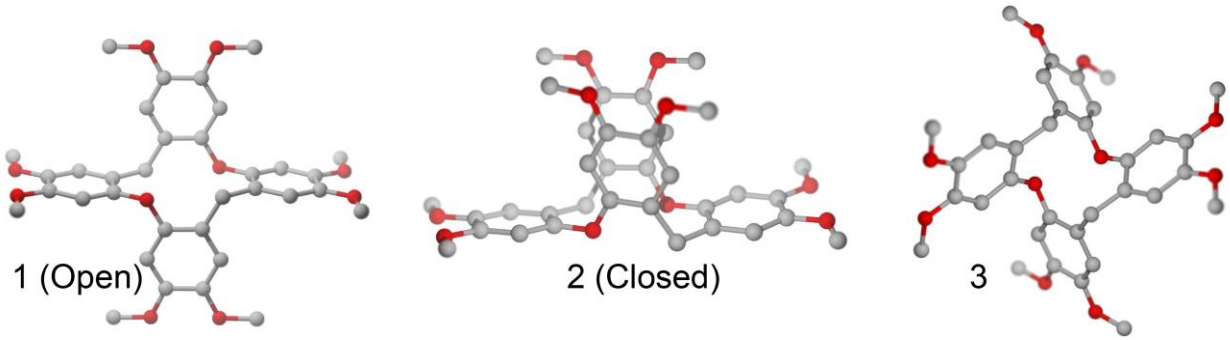

Table S4. The calculated relative energies (ΔE+ZPE), enthalpies (ΔH) and free energies (ΔG) of neutral $^{O\text{-}alt}$CTTV and cation radical $^{O\text{-}alt}$CTTV$^{\bullet+}$ using B2PLYPD3/BS2+PCM($CHCl_3$)//DFT/BS1+PCM($CHCl_3$) level to theory (in kcal/mol).

	ωB97XD	CAM-B3LYP-D3BJ	M062X
$^{O\text{-}alt}$**CTTV**			
1 (open)	0.0 (0.0) [0.0]	0.0 (0.0) [0.0]	0.0 (0.0) [0.0]
2 (closed)	0.6 (0.4) [2.1]	0.3 (0.2) [1.5]	1.7 (1.3) [3.9]
3	8.4 (8.4) [8.4]	8.7 (8.7) [8.7]	8.5 (8.5) [8.5]
$^{O\text{-}alt}$**CTTV**$^{\bullet+}$			
1 (open)	0.0 (0.0) [0.0]	0.0 (0.0) [0.0]	0.0 (0.0) [0.0]
2 (closed)	-9.0 (-9.1) [-7.7]	-9.4 (-9.5) [-8.1]	-8.8 (-8.9) [-7.3]
3	7.5 (7.0) [10.7]	4.9 (4.8) [5.5]	10.8 (10.8) [11.4]

Table S5. The calculated relative energies (ΔE+ZPE), enthalpies (ΔH) and free energies (ΔG) of cation radical $^{O\text{-}alt}$CTTV$^{\bullet+}$ using ωB97XD/BS1+PCM level to theory employing CH_2Cl_2, $CHCl_3$, CH_3CN and MeOH solvents (in kcal/mol).

$^{O\text{-}alt}$**CTTV**$^{\bullet+}$	CH_2Cl_2	$CHCl_3$	CH_3CN	MeOH
1 (open)	0.0 (0.0) [0.0]	0.0 (0.0) [0.0]	0.0 (0.0) [0.0]	0.0 (0.0) [0.0]
2 (closed)	-13.2 (-13.2) [-12.0]	-12.7 (-12.8) [-11.4]	-13.6 (-13.7) [-12.3]	-13.6 (-13.7) [-12.1]
3	-3.2 (-4.1) [0.7]	-2.7 (-3.2) [0.5]	-3.4 (-3.8) [-0.2]	-3.1 (-3.7) [-0.3]

Figure S10. The calculated spin density (isovalue 0.0004) of $^{O\text{-}alt}$CTTV$^{\bullet+}$ cation radical closed conformer using ωB97XD/BS1+PCM($CHCl_3$) side (left) and top (right) views.

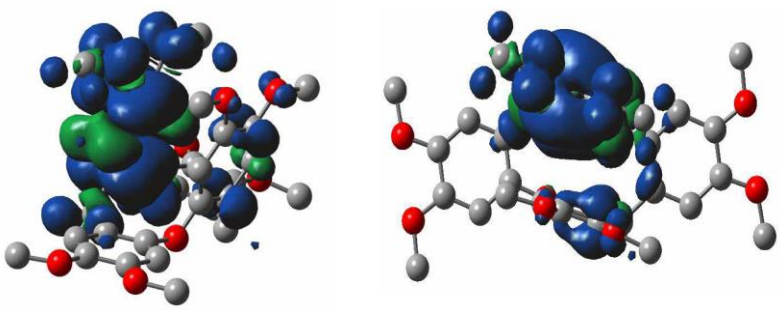

Figure S11. The calculated spin density (isovalue 0.0004) of CTTV$^{\bullet+}$ cation radical closed conformer using ωB97XD/BS1+PCM($CHCl_3$) side (left) and top (right) views.

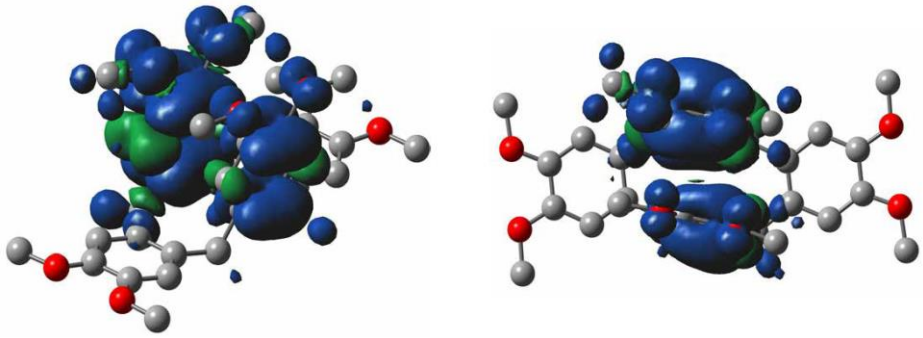

Table S6. Comparison of the calculated center-to-center distance (in Å) of cofacially veratrole moieties and the predicted UV-Vis band (in nm) in the near-IR region (NIR) of $^{O\text{-}alt}$CTTV$^{\bullet+}$ with experimental data. All calculated values are form the totally optimized geometries using BS1 and PCM($CHCl_3$).

	ωB97XD	CAM-B3lYP-D3BJ	M062X	Experimental
Center-to-center (Å)	3.44	3.46	3.41	3.43
Wavelength (nm)	1173.5	1213.0	1286.0	1850
Wavenumber (cm^{-1})	8521.2	8244.0	7776.0	5405.4

Figure S12. The simulated UV-Vis-NIR spectrum of $^{O\text{-}alt}$CTTV cation radical closed conformer using ωB97XD/BS1+PCM($CHCl_3$). The isovalue for HOMO and LUMO is 0.02. The calculated peak in the near-IR region is 1173.5 nm with the oscillator strength of 0.022 which the major contribution (96%) is from HOMO→LUMO.

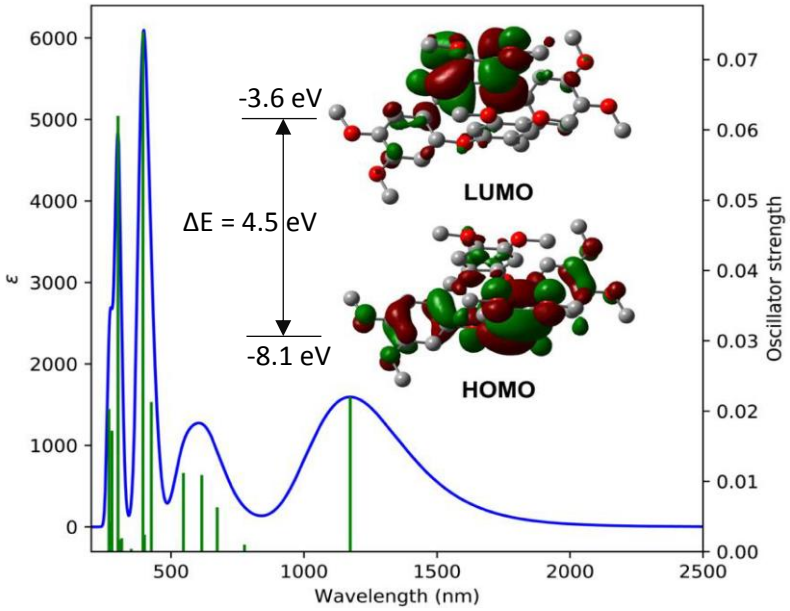

Figure S13. The simulated UV-Vis-NIR spectrum of CTTV cation radical closed conformer using ωB97XD/BS1+PCM($CHCl_3$). The isovalue for HOMO and LUMO is 0.02. The calculated peak in the near-IR region is 1476.2 nm with the oscillator strength of 0.071 which the major contribution (53%) is from HOMO→LUMO.

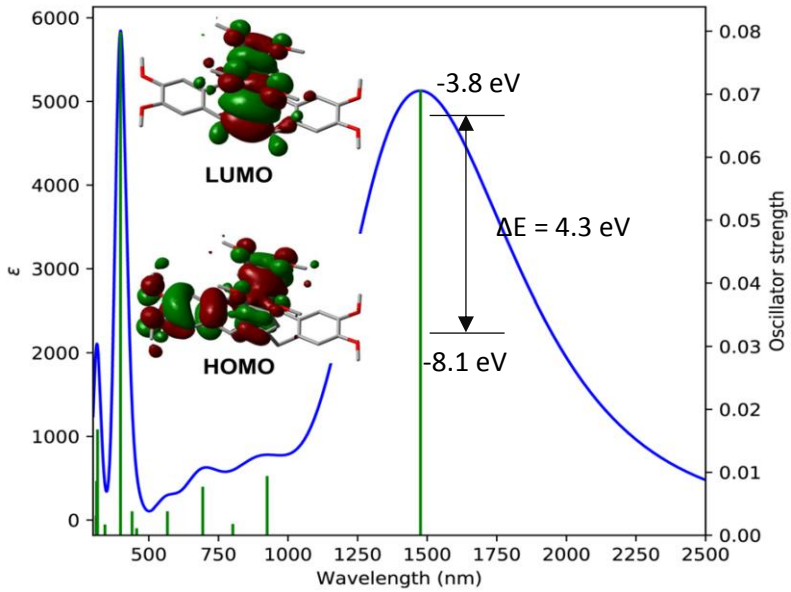

Table S7. Comparison of the experimental and calculated (scaled using TMS, see computational details) ^{1}H chemical shifts of open and closed conformers of $^{O\text{-}alt}$CTTV using ωB97XD/BS1+PCM($CHCl_3$).

Open	
Experimental	Calculated
6.76	6.89
6.37	6.60
4.29	4.18
3.87	3.80
3.72	3.61
3.17	3.06

Closed	
Experimental	Calculated
7.03	7.18
6.60	6.84
6.38	6.65
5.20	5.02
4.82	4.92
4.04	4.02
3.80	3.78
3.65	3.53
3.25	3.24
3.26	3.13

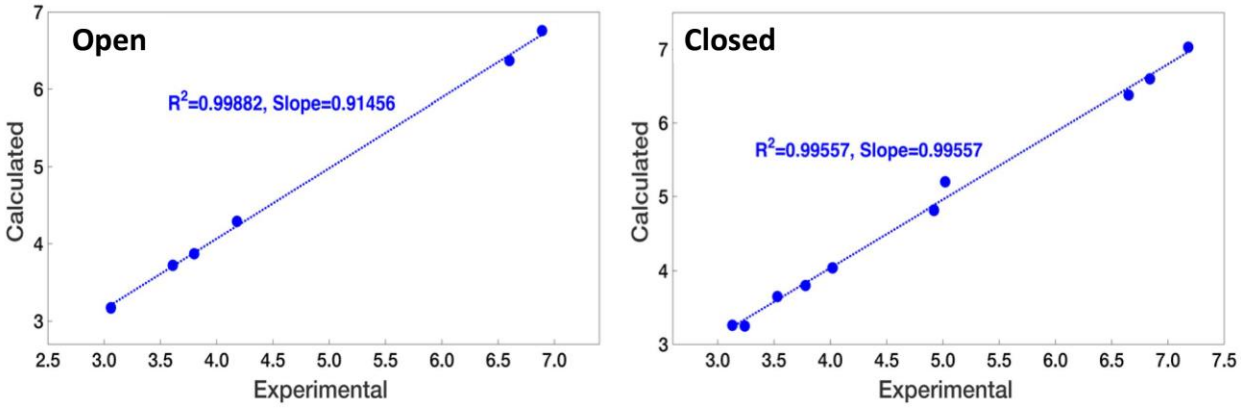

Figure S14. Linear correlation of experimental and calculated ^{1}H chemical shifts of open and closed conformers of $^{O\text{-}alt}$CTTV using ωB97XD/BS1+PCM($CHCl_3$).

S8. References

1) Engman, L.; Hellberg, J.; Ishag, C.; Söderholm, S. New alkoxylated dibenzo[1,4]dichalcogenines as donors for low-dimensional materials: electrochemistry and cation-radical salts. *J. Chem. Soc., Perkin Trans. 1*, **1988**, *0*, 2095–2101.
2) Gaussian 16, Revision B.01, Frisch, M. J.; Trucks, G. W.; Schlegel, H. B.; Scuseria, G. E.; Robb, M. A.; Cheeseman, J. R.; Scalmani, G.; Barone, V.; Petersson, G. A.; Nakatsuji, H.; Li, X.; Caricato, M.; Marenich, A. V.; Bloino, J.; Janesko, B. G.; Gomperts, R.; Mennucci, B.; Hratchian, H. P.; Ortiz, J. V.; Izmaylov, A. F.; Sonnenberg, J. L.; Williams-Young, D.; Ding, F.; Lipparini, F.; Egidi, F.; Goings, J.; Peng, B.; Petrone, A.; Henderson, T.; Ranasinghe, D.; Zakrzewski, V. G.; Gao, J.; Rega, N.; Zheng, G.; Liang, W.; Hada, M.; Ehara, M.; Toyota, K.; Fukuda, R.; Hasegawa, J.; Ishida, M.; Nakajima, T.; Honda, Y.; Kitao, O.; Nakai, H.; Vreven, T.; Throssell, K.; Montgomery, J. A., Jr.; Peralta, J. E.; Ogliaro, F.; Bearpark, M. J.; Heyd, J. J.; Brothers, E. N.; Kudin, K. N.; Staroverov, V. N.; Keith, T. A.; Kobayashi, R.; Normand, J.; Raghavachari, K.; Rendell, A. P.; Burant, J. C.; Iyengar, S. S.; Tomasi, J.; Cossi, M.; Millam, J. M.; Klene, M.; Adamo, C.; Cammi, R.; Ochterski, J. W.; Martin, R. L.; Morokuma, K.; Farkas, O.; Foresman, J. B.; Fox, D. J. Gaussian, Inc., Wallingford CT, 2016.
3) Zhao, Y.; Truhlar, D. G. The M06 Suite of Density Functionals for Main Group Thermochemistry, Thermochemical Kinetics, Noncovalent Interactions, Excited States, and Transition Elements: Two New Functionals and Systematic Testing of Four M06-Class Functionals and 12 Other Function. *Theor. Chem. Acc.* **2008**, *120*, 215–241.
4) Yanai, T.; Tew, D. P.; Handy, N. C. A New Hybrid Exchange – Correlation Functional Using The. *Chem. Phys. Lett.* **2008**, *393*, 51–57.
5) Chai, J.-D.; Head-Gordon, M. Long-Range Corrected Hybrid Density Functionals with Damped Atom–atom Dispersion Corrections. *Phys. Chem. Chem. Phys.* **2008**, *10*, 6615–6620.
6) Grimme, S.; Ehrlich, S.; Goerigk, L. Effect of the Damping Function in Dispersion Corrected Density Functional Theory. *J. Comput. Chem.* **2011**, *32*, 1456–1465.
7) Grimme, S. Semiempirical Hybrid Density Functional with Perturbative Second-Order Correlation. *J. Chem. Phys.* **2006**, *124*, 0–16.
8) Menon, A. S.; Radom, L. Consequences of Spin Contamination in Unrestricted Calculations on Open-Shell Species: Effect of Hartree-Fock and Møller-Plesset Contributions in Hybrid and Double-Hybrid Density Functional Theory Approaches. *J. Phys. Chem. A* **2008**, *112*, 13225–13230.
9) Cancès, E.; Mennucci, B.; Tomasi, J. A New Integral Equation Formalism for the Polarizable Continuum Model: Theoretical Background and Applications to Isotropic and Anisotropic Dielectrics. *J. Chem. Phys.* **1998**, *107*, 3032–3041.
10) Wolinski, K.; Hinton, J. F.; Pulay, P. Efficient Implementation of the Gauge-Independent Atomic Orbital Method for NMR Chemical Shift Calculations. *J. Am. Chem. Soc*. **1990**, *112*,8251–8260.
11) J. P. Foster and F. Weinhold, Natural Hybrid Orbitals. *J. Am. Chem. Soc*., **1980**, *102*, 7211–7218.
12) O'Boyle, N. M.; Tenderholt, A. L.; Langner, K. M. cclib: A library for package- independent computational chemistry algorithms. *J. Comp. Chem.*, **2008**, *29*, 839–845.